In situ Raman spectroscopy — a valuable tool to understand operating catalysts

Gerhard Mestl [*]

Fritz-Haber-Institut der Max-Planck-Gesellschaft, Abt. Anorganische Chemie, Faradayweg 4-6, 14195 Berlin, Germany

Abstract

Laser Raman spectroscopy (LRS) is one of the most powerful tools for the in situ study of catalytic materials and surfaces under working conditions. Raman characterizations can be carried out at temperatures as high as 1000 K and in controlled atmospheres. Modern high light-throughput spectrometers permit the recording of the whole spectral range from 100 to 4000 cm^{-1} at once and time resolutions in the subsecond regime for materials with high Raman cross-sections. Transient temperature or pressure response studies, e.g. pulse experiments with isotope labels, are thus possible, and kinetic and spectroscopic characteristics can be related. Modern quartz fiber optics render possible easy spectroscopic access to catalytic reactors of defined and well characterized operation conditions. Quantitative relation of real catalytic steady state operation, e.g. catalytic activity and selectivity, to changes in the catalyst structure is thus made possible.

Several in situ LRS studies are discussed including the characterization of supported and unsupported Mo-based catalysts, confocal Raman microspectroscopy of mixed MoVW oxide catalysts, oxygen exchange in Sb_2O_3/MoO_3 oxide physical mixtures elucidating the catalytic synergy effects, and active surface intermediates during oxidative coupling of methane, and NO and N_2O decomposition over Ba/MgO catalysts related to the catalytic reaction via transient pressure step experiments. © 2000 Elsevier Science B.V. All rights reserved.

Keywords: Raman spectroscopy; Raman microspectroscopy; Selective oxidation; Synergy effects; Oxygen exchange; Oxidative coupling of methane; NO and N_2O decomposition

1. Introduction

The general physics of laser Raman spectroscopy (LRS) is discussed only briefly because this is covered in depth in textbooks and recent review articles on LRS as applied to catalysis [1–7]. In this contribution, advantages of Raman spectroscopy and also its limitations, e.g. quantification problems, are outlined and compared to other vibrational techniques. Recent Raman studies of catalytic materials are discussed.

1.1. Theoretical background

Atomic movements in crystals are only allowed with defined phase relations giving rise to the vibrational modes of the crystal. These collective atomic movements are termed acoustic or optical phonons depending on the generation of a dipole moment during the vibration. Optical phonons take part in inelastic light-

[*] Tel.: +49-30-8543-4440; fax: +49-30-8543-4401.

E-mail address: mestl@fhi-berlin.mpg.de (G. Mestl).

scattering processes due to their induced dipole moment.

The interaction of electromagnetic radiation with matter leads to absorption and reflection and light-scattering processes. In Rayleigh scattering (Fig. 1), most scattered photons have the frequency identical to the incident ones. But a small part of the scattered light may have a higher or smaller energy than that of the incident light. This process is known as the Raman effect: the incoming photon excites the scattering matter from its electronic ground state into a virtual state, from which it relaxes under the emission of a Raman scattered photon of smaller or higher energy (Stokes or anti-Stokes scattering), depending on the initial and final vibrational levels.

These light-scattering processes can be understood within a classical model of the scattering process. Such a classical model can describe the observed Raman shifts. The intensity or line shape of Raman bands, however, can only be determined via quantum mechanical ab initio calculation of the Raman-scattering transition moment.

In a quantum mechanical picture of Raman scattering, the incoming photon either generates an excited phonon and therefore has a lower energy after the scattering process or it annihilates an excited phonon in the solid and thus has a higher energy after the scattering event (Fig. 2). This process can be understood as a series of three elementary steps:

Step 1: The incident photon is annihilated (absorbed) under the generation of the virtual electron hole — pair 1.

Step 2: The virtual electron — hole pair 1 generates or annihilates a phonon under the formation of the virtual electron hole — pair 2.

Step 3: The virtual electron hole — pair 2 recombines under the emission of the Raman scattered photon.
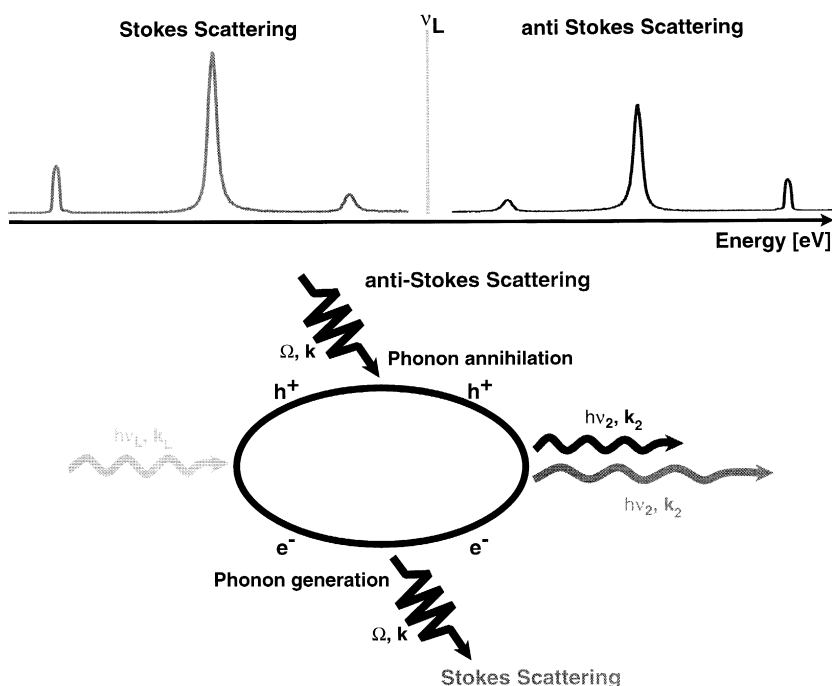

Fig. 1. Scheme of Stokes and anti-Stokes scattering relative to the excitation frequency (upper part). Scheme of the Raman scattering process in solid material (lower part).
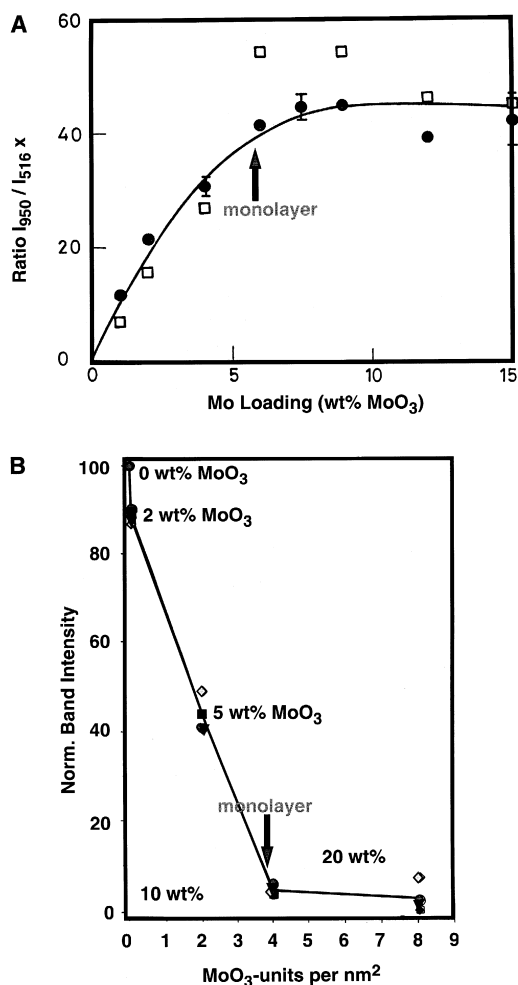
Fig. 2. (A) Intensity ratio of the Raman bands of the TiO_2 support at 516 cm^{-1} and the surface polymolybdate at 950 cm^{-1} as a function of Mo loading. (B) Raman band intensities of the TiO_2 support referenced to external Hg standard emission as a function of Mo loading (adapted from Ref. [7]).

Such ab initio calculations of these three combined processes in complex catalytic solids seem to be impossible with the necessary precision and, therefore, Raman spectral characterization is still done by comparison with reference spectra despite all the obvious disadvantages.

The Raman susceptibility, analogous to the classical model, describes the modulation of the electronic polarizability of matter by its lattice vibrations [8]. The Raman susceptibility can be developed as a Taylor series of the phonon wave vector:

$$\varepsilon(Q,\omega) = \varepsilon(\omega) + \frac{d\varepsilon(\omega)}{dQ}Q$$

$$+ 1/2\frac{d^2\varepsilon(\omega)}{dQ^2}Q^2 + \ldots, \qquad (1)$$

with ε the dielectricity constant, ω the frequency of the incident light and Q the phonon wave vector. The first term in Eq. 1 describes the first-order Raman scattering, and second term the second-order scattering process and so on. The interaction of an incident laser field and a phonon generates an induced dipole moment according to Eq. 2

$$P(\omega_L \pm \Omega) = \frac{d\varepsilon}{dQ}Q_0 E_L e^{-i(\Omega_L \pm \Omega)t}, \qquad (2)$$

with the $\pm$ sign assigning Stokes or anti-Stokes radiation. The intensity of the scattered radiation is proportional to ω_L^4 as described in Eq. 3:

$$I \propto \omega_L^4 \left|\frac{d\varepsilon}{dQ}\right|^2 \langle Q_0^2 \rangle, \qquad (3)$$

with $\langle Q_0^2 \rangle$ being the Boltzmann distribution. This ω^4-law explains the advantage of using high excitation frequencies: the higher the excitation frequency the higher the Raman scattered intensity.

High excitation frequencies lead to a second important advantage when conducting high temperature in situ Raman experiments: the higher the excitation frequency, the less is the black body radiation background. Raman spectra of lattice phonons can be recorded of operating catalysts under optimum conditions at temperature as high as 1000 K.

Furthermore, the sample temperature can be calculated from the measured intensities of a Stokes — anti-Stokes experiment from the term including the Boltzmann.

Eq. 3 of the Raman-scattering process relates the electronic system, expressed in ε, with the lattice vibrations, Q. At the proximity of pro-

nounced structures in ε, e.g. absorption bands, one obtains pronounced structures in $d\varepsilon/dQ$. Thus, effects in Raman scattering can be understood, which are due to resonant absorption of photons.

With this background, it is evident that Raman scattering provides much more information on a material than just the molecular vibrations. Information can also be obtained about the electronic nature of the material under study, e.g. defect centers like reduced transition metal ions.

Advantages of Raman spectroscopy relative to infrared techniques arise from the usually negligible gas phase scattering. In situ Raman spectra of active catalysts can be recorded without interference of the gas phase. In infrared spectroscopy, gas phase absorptions often complicate the measured spectra or render the experiment impossible.

Glass is a very weak Raman scatterer allowing a simple construction of in situ Raman cells. In IR spectroscopy, usually KBr windows have to be used for cells with all their limitations: water sensitivity, which makes purged spectrometers and cells necessary; low melting point, thus cooling of the cell windows is necessary in high temperature experiments; and the cut-off at about 450 cm^{-1}, which makes it difficult to record the internal vibrations.

Due to the fact that simple in situ Raman quartz reactors can be used, catalysts can be studied by LRS at very high temperatures. Especially, when a high frequency excitation line is used, black body radiation does not necessarily overwhelm the Raman scattered light. High temperature IR spectroscopy, however, is rather limited due to sample emission, and infrared emission spectroscopy is less well developed yet. Moreover, in situ Raman reactors can be designed closely matching typical plug flow reactors. Such an in situ reactor can have two catalyst beds, which allows the recording of the Raman spectrum on the surface of the second bed. By this approach, information is obtained on the catalysts structure under real steady state conditions inside the bed and not at the outer surface, which is always in contact with fresh gas phase. Additionally, the variation of the first catalyst bed height allows the determination of the working catalyst structure as function of contact time.

Typical high surface-area supports, e.g. silica or alumina, are weak Raman scatterers, but strongly absorb in the IR below 1200 cm^{-1}. Therefore, their Raman spectra usually do not overwhelm those of the supported metal oxides, which can be recorded down to approximately 50 cm^{-1}. These typical supports, however, are strong IR absorbers.

Water is a very weak Raman scatterer, but it has very intense IR absorptions. Raman spectroscopy, thus, can be conducted of aqueous solutions or suspensions. Adsorption processes of transition metal ions on supports or crystallization processes like the formation of zeolites can be characterized in situ.

The recently developed confocal Raman microspectroscopy technique allows the recording of Raman spectra with a spatial resolution of about 700 nm. This technique renders possible the determination of structural inhomogeneities in catalyst materials, and its correlation with elemental inhomogeneities as determined EDAX mapping. Recently even higher spatial resolutions of 100 nm were reached using near field optical microscopes [9].

2. Limitations

Some major problems may arise when recording Raman spectra of catalyst materials.

(i) Laser heating could lead to loss of hydration water, phase transitions, partial reduction or even complete decomposition and, thus, to artificially changed samples. Laser heating can be reduced by applying low laser powers (< 10 mW), cooling with an inert gas of high thermal conductivity, cylindrical lens foci [10], and rotating sample [11] or focussing lens [12,13] techniques, which decrease the energy flux [20]. The temperature at the laser focus can be calcu-

lated from the Stokes–anti-Stokes intensity ratio via Eq. 3 if the spectrometer function is precisely determined and the scanning multichannel technique is used [14–16].

(ii) Flourescence can overwhelm the Raman spectrum, which may be due to organic impurities, basic surface OH groups, proton superpolarizability or reduced transition metal ions when resonantly excited. Flourescence problems can be often solved by simply burning-off the organic contaminants or dehydroxylating the surface, if the sample tolerates these treatments. Changing the excitation frequency may also lead to fluorescence reduction. Thus, the application of FT Raman [17,18] systems or the recently developed UV Raman technique [19] may help, although excitation in the NIR (FT Raman) sometimes can cause fluorescence when reduced transition metal ions are present, and excitation in the UV may lead to unwanted photochemical reactions. Frequency modulation Raman spectroscopy [7] can also reduce the background because the spectrum is recorded as the first derivative.

(iii) The Raman scattering has an inherently low sensitivity due to the small Raman scattering cross-sections as compared to IR absorption coefficients. The low sensitivity can be somewhat improved increasing the excitation frequency due to the ν^4 law, one of the main advantages of UV Raman excitation. A technical solution to the problem of low sensitivity was found in the highly sensitive CCD cameras [21] and in high performance, holographic notch filters [22] to cut off the very intense Rayleigh scattering. These two inventions considerably improved the spectrometer technology: triple stage spectrometers, necessary for stray light reduction, with low light throughput now can be avoided. This led to an increase in measured intensity of about 10^2. This new generation Raman spectrometers [23,30] also allow for time-resolved experiments due to their high sensitivity and long-time stability. The latter is due to the fact that any moving parts, such as spectrographs, are avoided. The long-time stability

of this new spectrometer type is guaranteed too by the use of diode-pumped solid state lasers, which have a long-time stability of about 3%. This combination of spectrometer design and long-time stable laser renders possible the recording of Raman spectra over extended time periods without changes in the experimental baseline.

Quantitative Raman spectroscopy is the most difficult task due to the inherently unknown Raman-scattering cross-sections. The Raman-scattering cross-section even of pure components may change as a function of temperature, pressure or reaction conditions. Moreover, Raman cross-sections of surface species, like adlayers or adsorbates, cannot be compared with reference data of pure compounds due to a possible, unknown electronic effect of the support even when their structure remained unchanged relative to the reference.

The surface enhanced Raman-scattering effect (SERS) [30], observed on certain metal surfaces, like Al, Cu, Ag, and Au, leads to an enhancement of the cross-section of adsorbed surface species by a factor of 10^6 as compared to the unsupported reference.

Raman intensities of surface species on oxidic supports do not always show a linear dependency with concentration (Fig. 2A). Quincy et al. [25] observed that the ratio of the band of the surface Mo species at 950 cm^{-1} and that of the anatase support at 516 cm^{-1} increased up to monolayer coverage to level off at higher loadings. A relative Raman cross-section of MoO_3 of 3.6 was determined from the relative ratio of the surface molybdate bands and the bands due to MoO_3. This relative Raman cross-section was determined to be 17 for alumina-supported samples by referencing to KNO_3 [26]. These different relative scattering efficiencies were attributed to an altered scattering efficiency for titania-supported surface species. A physical theory of this changed Raman cross-section, however, is not available to date.

More recently, the relative Raman band intensities of Mo species and titania support were

referenced to external Hg emission. The calibration to Hg emission revealed a decrease of the support bands, beside increasing Mo intensities, with increasing Mo loadings already below monolayer coverage. Above monolayer coverage, which is reached at a Mo loading of 4 MoO_3 units/nm^2 (10 wt.% MoO_3), the relative intensity of the titania bands remained constant (Fig. 2B) [7]. A modification of the support surface polarizability induced by the Mo overlayer was suggested to be the physical reason for that, because the incident light penetrates much deeper into the sample. Such an unexpected decrease of support bands below monolayer coverage was also observed by others for ZrO_2, Nb_2O_5, and CeO_2 supports [7]. The physical background of this behavior of the Raman-scattering efficiency of support materials is not understood to date.

Raman intensities of supported transition metals oxides may change as a function of treatment. Reduction, for example, generally leads to colored samples, which have a higher absorption coefficient. Thus, the intensity of the Raman scattered light can be strongly reduced when self-absorption occurs. The measured Raman intensity cannot be directly related to the concentration of a certain transition metal surface species.

In summary, quantification of Raman spectra by comparison of relative peak intensities must be considered with care and may lead to erroneous results because the absolute or even relative Raman-scattering efficiencies are unknown or cannot be determined precisely enough. The determination of the relative Raman cross-sections of pure, optically homogeneous samples is already extremely difficult. This determination seems to be impossible for heterogeneous, polydisperse materials. Intolerable errors may arise from unavoidable inhomogeneities in powder mixtures due to different particle sizes and morphologies. Large particles of phase A may, for example, be encapsulated by small particles of phase B. The laser beam may preferentially hit one or the other component in such samples.

Additionally, particle aggregation or disintegration may occur during in situ treatments leading to changes of the Raman intensity being a function of particle size. Furthermore, the scattering volume is considerably reduced for opaque materials due to damping of the incident and scattered light. In summary, a precise determination of the scattering volume seems to be impossible.

Moreover, it is not necessary to point out that the spectrometer function has to be precisely determined for an attempt to collect the physically correct Raman intensities [14,15]. Summarizing, the quantification of Raman spectra of heterogeneous catalysts must be considered with care and may prove impossible within reasonable limits of accuracy.

3. Molybdenum-based catalysts

3.1. Oxygen exchange in MoO_3 / Sb_2O_4-selective partial oxidation catalysts

Selective partial oxidation reactions are suggested to proceed via the Mars–van Krevelen mechanism: so-called ''lattice'' oxygen of the catalyst is incorporated into the reactant in one step of the catalytic cycle; the oxygen vacancy is reoxidized by gas phase oxygen in the second step.

The remote control mechanism of multiphase-selective partial oxidation catalysts assumes that gas phase oxygen is activated on the donor phase [27]. The activated oxygen is then suggested to spill over onto the acceptor phase, at which it is (re)generating the catalytically active sites. This mechanism is suggested to explain the experimentally observed synergisms in multiphase catalysts.

Mixed MoO_3/Sb_2O_4 catalysts show such a pronounced synergy in selective partial oxidation. Sb_2O_4 is considered to be the donor, while MoO_3 acts as the catalytically active acceptor. In situ Raman spectroscopy was applied in order to characterize the reaction of $^{18}O_2$ with the

donor, the acceptor, and their physical mixtures [28–30].

These in situ Raman experiments proved that no detectable ^{18}O exchange occurred for the pure stiochoimetric oxides up to 750 K. ^{18}O incorporation was only detected for partly reduced MoO_{3-x}. Spectrum (a) of Fig. 3A shows the Raman spectrum of stoichiometric MoO_3, whereas spectrum (b) of Fig. 3A shows the in situ Raman spectrum after evacuation to 10^{-1} Pa. The dramatic reduction of the MoO_3 Raman intensities, i.e. S/N ratio, proves that the Raman cross-section of substoichiometric MoO_{3-x} is much smaller as that of MoO_3. The pronounced decrease of the band intensities at 660

and 818 cm^{-1} relative to the band at 990 cm^{-1} suggests a preferential loss of oxygen from Mo−O−Mo bridges (along the c-axis) and the long terminal Mo=O groups along the a-axis than from the short terminal Mo=O groups along the b-axis.

The observed new band at 888 cm^{-1} is in the frequency regime of tetrahedrally coordinated Mo. It is known that Mo centers at the shear planes of Mo suboxides are fourfold coordinated. Therefore, the new band at 888 cm^{-1} is attributed to Mo−O vibrations of the shear defects in MoO_{3-x}.

^{18}O incorporation was proven by Raman bands at 648, 793, and 948 cm^{-1} after this
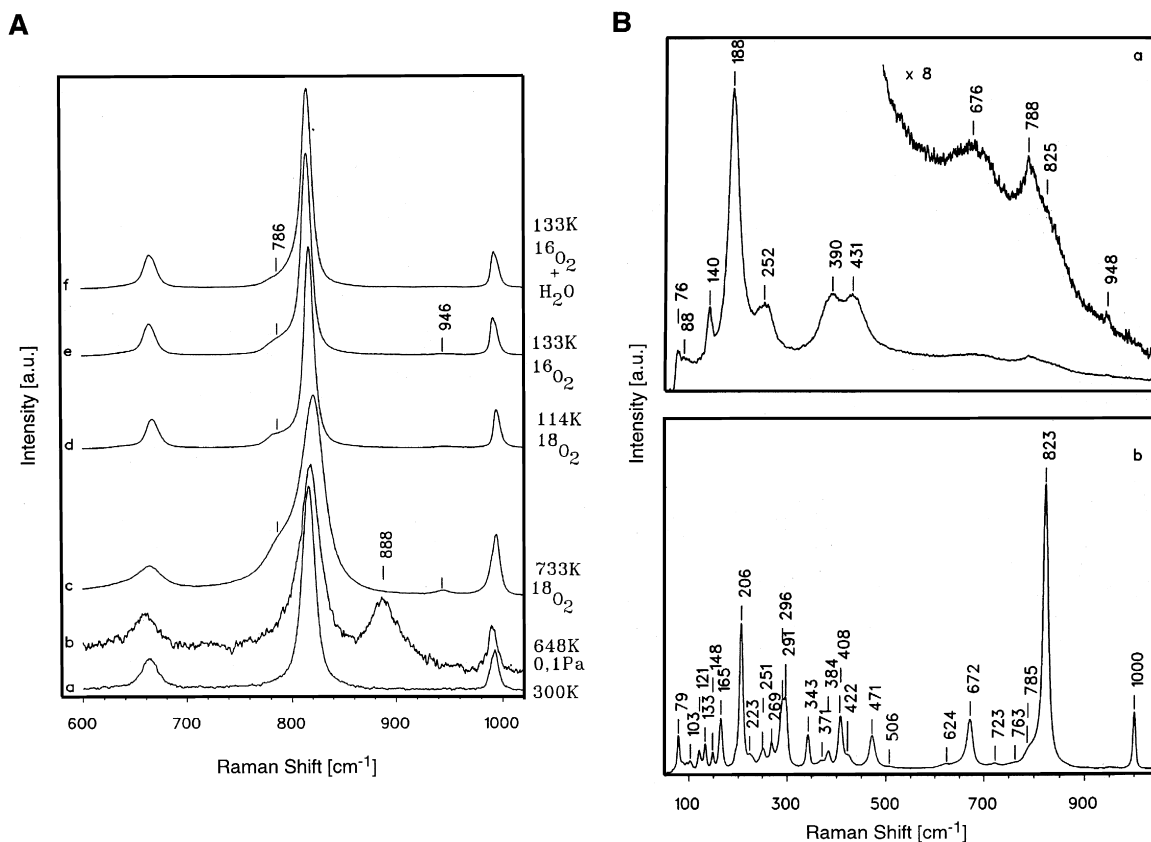

Fig. 3. (A) In situ Raman spectra of MoO_3 recorded during ^{18}O-exchange experiments: MoO_3 as received (a), after evacuation to 0.1 Pa at 648 K (b), after ^{18}O-reoxidation at 733 K (c), at 114 K (d), after additional oxidation in $^{16}O_2$, recorded at 133 K (e), and after additional oxidation in $^{16}O_2/H_2O$, recorded at 133 K (f) (adapted from Ref. [28]). (B) In situ Raman spectra of the physical mixture of MoO_3 and Sb_2O_4 (50:50) recorded during ^{18}O-exchange experiments: (a) high temperature (733 K) Raman spectrum after evacuation to 0.1 Pa at 648 K and subsequent ^{18}O-reoxidation at 733 K, (b) low temperature (114 K) Raman spectrum after evacuation to 0.1 Pa at 648 K and subsequent ^{18}O-reoxidation at 733 K (adapted from Ref. [30]).

sample was calcined in $^{18}O_2$ and the simultaneous disappearance of the defect band (spectrum c) of Fig. 3A), hence, oxygen vacancies in oxygen-deficient MoO_{3-x} could be replenished. Re-exchange of ^{18}O with $^{16}O_2$ was not possible, even not in presence of H_2O (spectra d) and e) of Fig. 3A). Oxygen incorporation only occurs when oxygen vacancies are present (substoichiometric MoO_{3-x}), direct oxygen exchange could not be detected under the experimental conditions. A comparison of the ^{18}O labeled band intensities confirmed that the terminal Mo=O groups having the highest bond order were less exchanged relative to the Mo=O groups along the *a*-axis and the Mo−O−Mo bridges.

The physical mixture of MoO_3 and Sb_2O_4 (Fig. 3B), mounted on the same sample holder, was identically treated, but did not lead to a more pronounced ^{18}O incorporation as compared to pure MoO_3 (spectrum b) of Fig. 3B). A comparison of the high temperature (spectrum a) of Fig. 3B) and the low temperature spectrum (spectrum b) of Fig. 3B) reveals a dramatic reduction of the Raman-scattering cross-section of crystalline MoO_3 at high temperatures relative to Sb_2O_4. This unambiguously confirms the problems that occur when one attempts to quantify Raman spectral data. From these experiments, it was concluded that (a) only oxygen vacancies can be replenished by oxygen incorporation, direct O-exchange does not occur, (b) oxygen exchange between donor and acceptor in the physical mixture via bulk diffusion is excluded, and (c) oxygen spillover, if present, remains below the Raman detection limit.

3.2. High temperature in situ Raman characterization of supported Mo catalysts

The Raman spectra of supported Mo catalysts change depending on the Mo loading. Ambient Raman spectra of low loaded catalysts show the presence of monomolybdates. Heptamolybdates are detected for intermediate loadings, and MoO_3 is found for highly loaded materials (Fig. 4A). This picture of surface species, however, dramatically changes when in situ Raman spectra are recorded at high temperatures under controlled conditions [31]. In Fig. 4B, the Raman spectral changes are shown of supported Mo catalyst when the material is heated in dry oxygen at 633 K. The spectrum of heptamolybdate-like surface species has disappeared and a new band appears at 1006 cm^{-1}, indicating the presence of a very distorted Mo species. This new band is attributed to surface monoxo species of still discussed symmetry. This in situ experiment clearly demonstrates the absolute necessity of controlling the experimental conditions. The structure of surface species is strongly affected by the degree of hydration. Surface mono- and polymolybdates form isolated, strongly distorted monooxo species. In this context, it must be noted that uncontrolled dehydration in the laser spot may have happened in earlier Raman studies.

3.3. Raman characterization of the spreading of MoO_3 over Al_2O_3

The XRD reflections of MoO_3 disappear with the time when a physical mixture of MoO_3 and Al_2O_3 is calcined at 700 K in air [32]. XPS and ISS [33], EXAFS [34], and Raman [35–37] studies revealed that a MoO_3 monolayer was formed on Al_2O_3 during this treatment. Different surface species were detected, depending on the presence of water vapor. Crystalline MoO_3 was observed under dry conditions, whereas heptamolybdates were detected in presence of water vapor. Thus, two processes were identified, the actual spreading of MoO_3 over the support surface, and its transformation into surface polymolybdates in presence of H_2O. Knözinger and Taglauer [38,39] developed the so-called unrolling-carpet mechanism, which was suggested to be driven by the reduction of the interface free energy of the system MoO_3/Al_2O_3.

Raman microscopy with a lateral resolution of about 2 μm was further used to characterize the spreading of MoO_3 across-Al_2O_3. Wafer
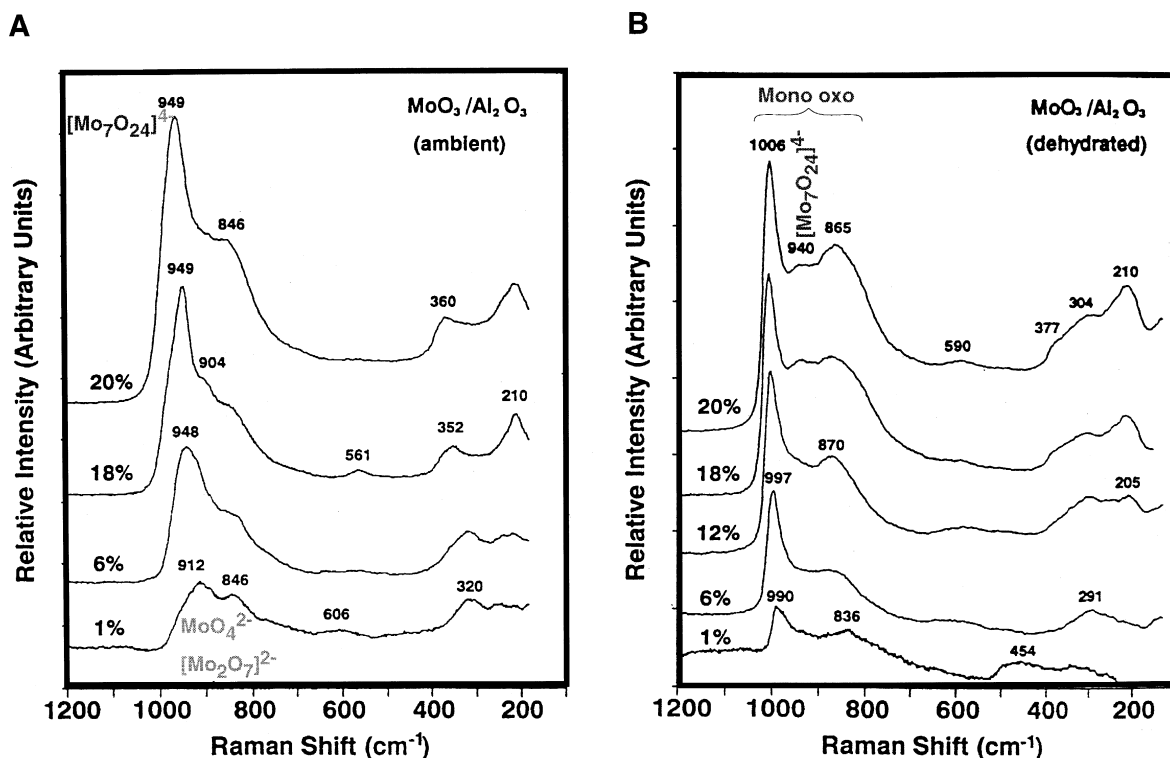
A

B

Fig. 4. (A) Raman spectra of Mo/Al$_2$O$_3$ catalysts as a function of Mo loading recorded under ambient conditions. (B) In situ Raman spectra of Mo/Al$_2$O$_3$ catalysts as function of Mo loading recorded after dehydration (adapted from Ref. [31]).

specimen were prepared from Al$_2$O$_3$ and MoO$_3$ having a sharp dividing line between the two phases (Fig. 5) [35]. After calcination in dry oxygen at 800 K for 100 h, MoO$_3$ Raman signals were detected on Al$_2$O$_3$ at distances as far as 500 μm from the former phase boundary. After calcination in moist oxygen, polymolybdate Raman bands were observed up to a distance of 1 mm from the original phase boundary. Raman microscopy clearly proved that spreading of MoO$_3$ occurred over macroscopic distances, and that H$_2$O led to a change in the structure of the surface species.

3.4. In situ Raman characterization of the spreading over Al$_2$O$_3$

In Fig. 6, in situ Raman spectra are depicted of a physical mixture of 9 wt.% MoO$_3$ and Al$_2$O$_3$, which were recorded at 823 K in dry oxygen (a) and after quenching to room temperature (b) [37]. It is evident that the Raman spectrum of crystalline MoO$_3$ was completely lost at a temperature more than 250° lower than its melting point (1086 K). The spectrum (a) has completely lost any structure in the lattice mode regime. Therefore, this spectrum is attributed to the spreading species. The frequency determined for the terminal Mo=O bonds comparable to those of crystalline MoO$_3$ suggests that the spreading species are small oligomer fragments of the MoO$_3$-tetrahedral chains in MoO$_3$ [40]. During quenching to room temperature (spectrum (b)), recrystallization seems to occur to some extent, and this spectrum may be attributed to disordered "glassy" MoO$_3$.

In summary, it seems to be proven that MoO$_3$ melts at its surface at about its Tammann temperature as suggested by the unrolling carpet mechanism. Small (MoO$_3$)$_x$ oligomers spread
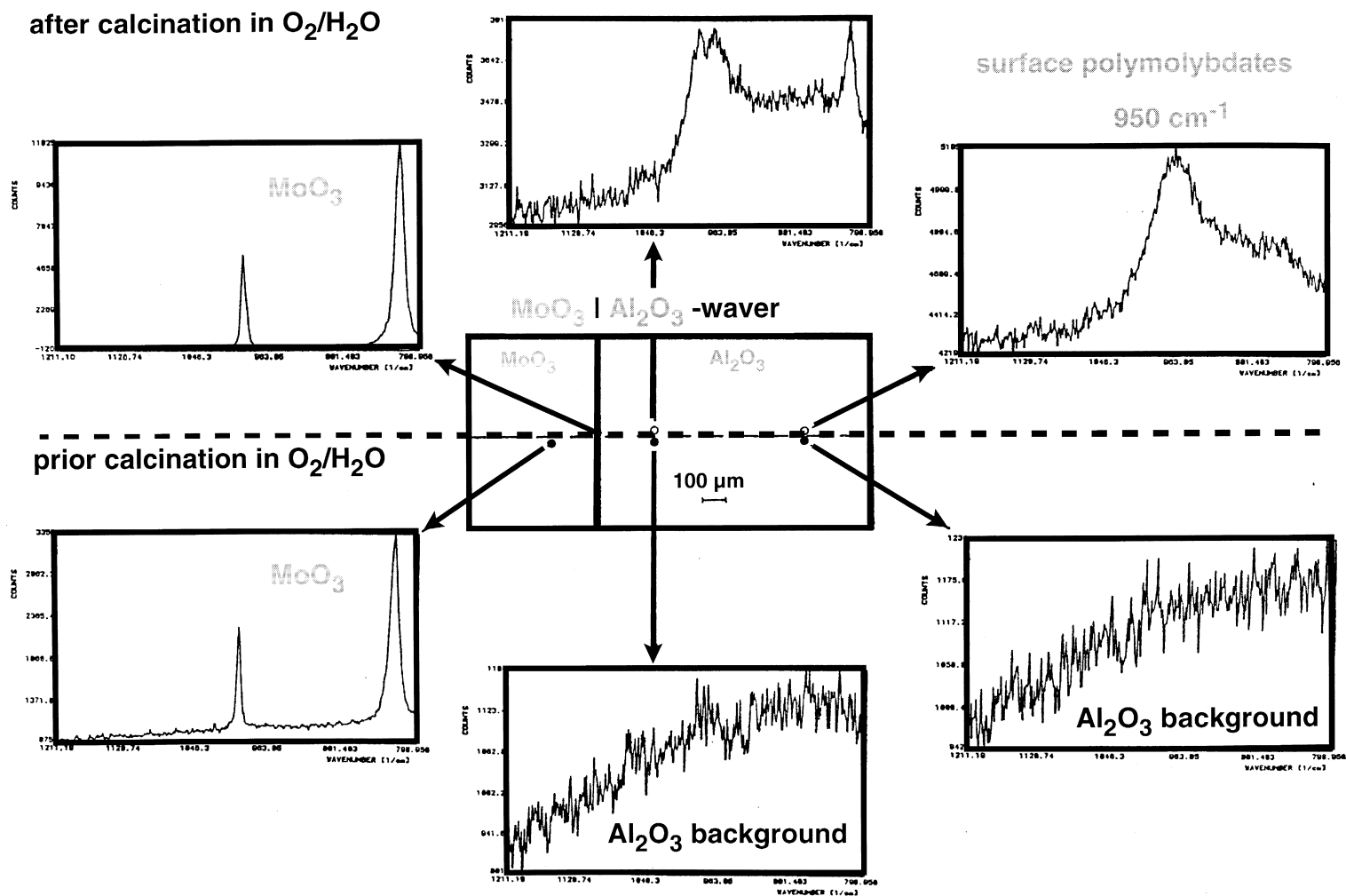
after calcination in O$_2$/H$_2$O

MoO$_3$

surface polymolybdates

950 cm^{-1}

MoO$_3$ | Al$_2$O$_3$ -waver

MoO$_3$ Al$_2$O$_3$

prior calcination in O$_2$/H$_2$O

MoO$_3$

100 µm

MoO$_3$

Al$_2$O$_3$ background

Al$_2$O$_3$ background

Fig. 5. Conventional Raman microspectroscopy of the spreading of MoO$_3$ across an Al$_2$O$_3$ waver after calcination in O$_2$ /H$_2$O: Raman spectra of the waver prior to any treatment (lower part), Raman spectra of the waver after calcination (upper part) (Adapted from Ref. [35]).
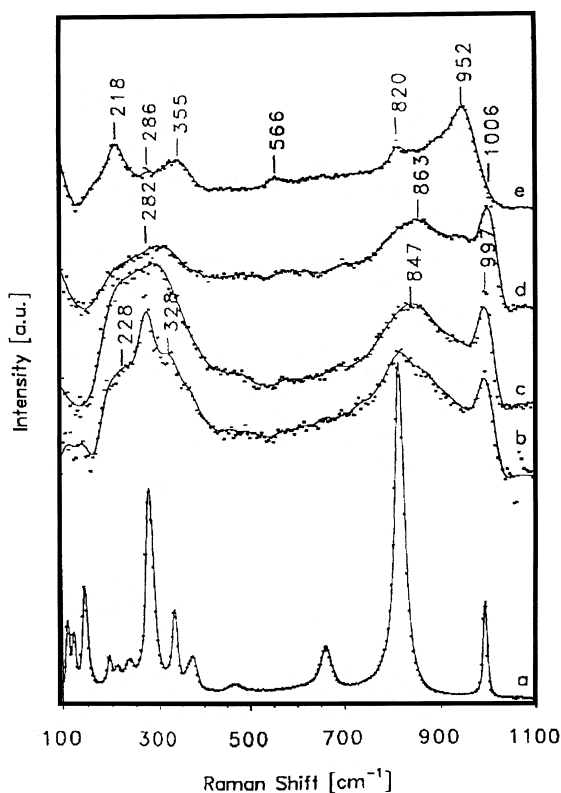
Fig. 6. In situ high temperature Raman spectra of a physical mixture of MoO₃ (9 wt.%) and Al₂O₃ during calcination in O₂ at 723 K (a), at 813 K (b), 823 K (c), after rapid quenching to 298 K (d), and after rehydration at 298 K in air (e) (adapted from Ref. [36]).

over Al_2O_3 driven by the reduction of the surface free energy of the overall system. Recrystallization to MoO_3 may occur in dry oxygen, hydrolyzation and rearrangment to polymolybdates in presence of H_2O.

3.5. Confocal Raman spectromicroscopy of mixed oxide catalysts

The spatial resolution of conventional microscopy is theoretically limited by the diffraction limit as defined by the wavelength of the light used, practically by imperfections of optical parts. To increase the spatial resolution to the theoretical diffraction limit, a pin hole is put into the light path in confocal microscopy [41]. By adjusting the pin hole size, light is collected on the detector, which is reflected from an area

determined by the diffraction limit, e.g. about 700 nm when an excitation frequency of 632 nm is used.

Molybdenum-based mixed oxide catalysts are widely used in selective partial oxidation reactions. Pure MoO_3-based catalysts exhibit also high selectivities to formaldehyde but with reduced methanol conversions [42]. SEM-EDX mapping [43] revealed an inhomogeneous element distribution in a mixed oxide catalyst containing Mo, V and W. XRD of the mixed oxide only showed amorphous patterns, which could be simulated with two components, amorphous MoO_3 and amorphous Mo_5O_{14}. Confocal Raman mapping was performed in order to characterize structural variations in the catalyst, which may arise from the varying transition metal concentrations. A set of 1000 Raman spectra was recorded within an area of 30 times 30 μm. Fig. 7A shows three experimental spectra, which show the extreme spectral differences within this data set. In all spectra, the characteristic Raman spectrum of orthorhombic α-MoO_3 with bands at 666, 820 and 995 cm^{-1} was absent in agreement with XRD. Instead bands were detected at 995, 985, 850, 815 and 770 cm^{-1}. All three transition metals, Mo, V and W, however, have Raman bands in this frequency regime depending on their coordination sphere and symmetry. Therefore, a straightforward assignment of the detected bands to certain species is not possible.

Statistical analysis was used to obtain further structural details of the MoVW mixed oxide catalyst. Chemometry is a fast developing field in analytical chemistry, which uses mathematical and statistical tools to plan and optimize measurements and experiments. Maximum information is obtained from data sets by statistical data reduction to independent principal components (PCs). The experimental spectra, thus, can be recalculated from the determined PCs by a linear combination according to:

$$Spectrum_n = c_{n_1}PC_{n_1} + c_{n_2}PC_{n_2} + \cdots + c_{n_m}PC_{n_m}, \qquad (4)$$
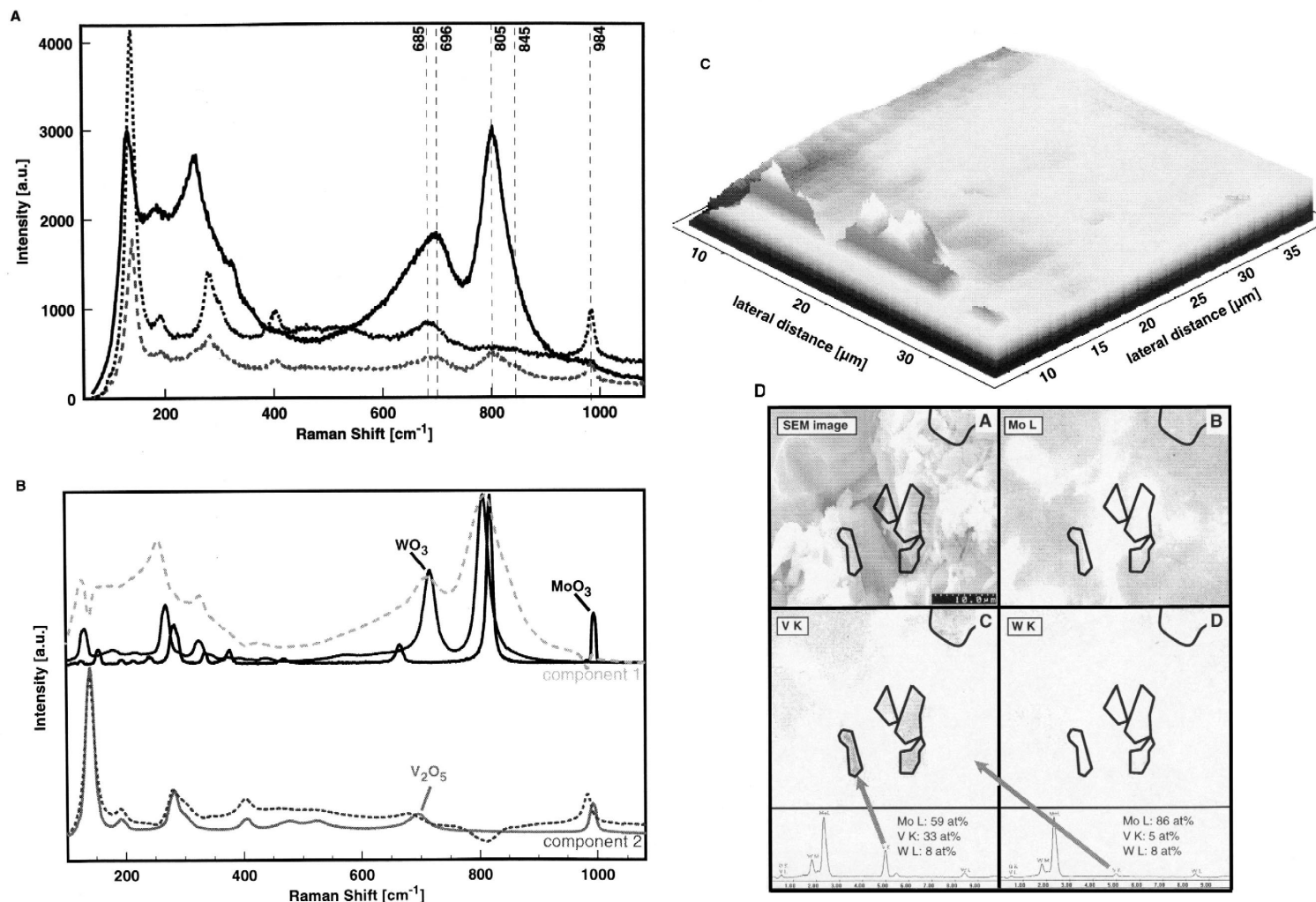
Fig. 7. Confocal Raman microspectroscopy (30×30 μm) of a MoVW mixed oxide catalyst. (A) Three characteristic Raman spectra of a set of 1000 spectra recorded laterally resolved proving drastic structural inhomogeneities. (B) Simplissma analysis of the set of 1000 Raman spectra revealing the presence of two independent principal spectral components in the sample (dashed lines). The Raman spectra of the MoO_3, WO_3, and V_2O_5 references are shown as solid lines. (C) 3D plot of the Raman intensity ratio of the bands at 805 and 845 cm^{-1} indicative for the two independent principal components in the sample proving spatial inhomogeneity. (D) SEM-EDX mapping of a similar area (30×30 μm) proving inhomogeneous V distribution relative to Mo and W.

with c_{n_i} the weight (or coefficient) of the n_ith PC. Thus, chemometric data reduction is identical to finding the eigenvalues of the coefficient and PC matrix.

From this set of 1000 Raman spectra, two PCs could be calculated. The two PCs together with the Raman spectra of single crystalline MoO_3, WO_3 and V_2O_5 are displayed in Fig. 7B. Component 1 (upper spectrum of Fig. 7B) shows a close resemblance to the spectra of MoO_3 and WO_3 (solid line, Fig. 7B), suggesting a structure related to MoO_3, e.g. a suboxide of the MoO_3-type with crystallographic shear planes. The band at 995 cm^{-1} may be assigned to terminal $Mo=O$ vibrations along the (010) lattice direction in α-MoO_3 [30]. The band or shoulder at 815 cm^{-1} can be attributed to $Mo=O$ stretches along the (100) lattice direction in α-MoO_3 [30], while the shoulder at 665 cm^{-1} may arise from the symmetric stretching vibration of the $Mo-O-Mo$ bridges along the (001) direction. Crystalline WO_3 has its major Raman bands at 808 and 714 cm^{-1}. XRD of this material excludes the presence of crystalline WO_3 as a separate phase, but tungsten can be isostructurally substituted in MoO_3. Therefore, the asymmetry of the band at 813 cm^{-1} toward lower frequencies and the band observed at about 710 cm^{-1} may arise from WO_6 units in the MoO_3-type mixed suboxide. XRD identified a component of the MoO_3-type structure in the MoVW mixed oxide catalyst. The first Raman spectral component, thus, may be related to the structure of this $MoWO_{3-x}$ suboxide mainly containing Mo and W.

V_2O_5 exhibits Raman bands in this frequency regime at 997 and 703 cm^{-1} [44]. XRD excludes the presence of crystalline V_2O_5 as a separate phase in the MoVW mixed oxide. Therefore, the spectral features at 995 and 710 cm^{-1} cannot be assigned to crystalline V_2O_5.

The second component (lower spectrum of Fig. 7B) shows a completely different spectral distribution with main features at 985, 773, 400, 275 and 90 cm^{-1}. This second component closely resembles the Raman spectrum of V_2O_5 suggesting that this component must be identified with the amorphous V_2O_5 contribution in the XRD patterns.

In Fig. 7C, the intensity ratios are shown as calculated for the intensity ratios between the bands attributed to the amorphous MoO_3-type suboxide and the amorphous V_2O_5-type oxide. Each pixel of the plot represents one confocal Raman spectrum of the mixed oxide specimen. The different intensity ratios obtained for the metal-oxygen vibrations clearly evidence that the sample is structurally heterogeneous. Thus, elemental heterogeneity as detected by SEM-EDX mapping (Fig. 7D) leads to structural heterogeneity.

A comparison of the spatial element distributions and the Raman spectral distributions reveals that the MoO_{3-x}-type and the V_2O_5-type oxides are exclusively formed. If the tentative band assignment were correct, the MoO_{3-x}-type suboxide is preferentially formed in those small sample areas with a high V concentration, whereas the V_2O_5-type oxide is formed in the remaining areas with a homogeneous Mo and W distribution.

4. Ba/MgO catalysts for NO and N_2O decomposition

NO can be directly decomposed into N_2 and O_2 on barium oxide supported on MgO. This catalyst exhibits a very unusual activity pattern depending on the reaction temperature [45]. For Ba loadings > 11 mole%, the catalytic steady state activity shows a sharp maximum. This maximum activity depends on the partial pressures of NO and O_2. Time resolved in situ LRS permitted to elucidate this unusual behavior on the basis of various surface phases and their surface chemistry [46–48].

Depending on operation conditions, Raman spectra were recorded of several different $Ba-NO_x$ species in the catalyst material, including barium nitrate $Ba(NO_3)_2$, barium nitrite $Ba(NO_2)_2$, and a barium nitro species — bar-

ium oxide with a nitro (NO_2) ligand at the barium. The reaction parameters gas partial pressures and temperatures were varied around the activity maximum to explore the relationship between a probable intermediate and the rate of reaction. In situ Raman spectroscopy provided information on the complex activation behavior of $Ba(NO_3)_2$ (Fig. 8A). Crystalline $Ba(NO_3)_2$ (phase I) was present after impregnation and drying. The crystalline $Ba(NO_3)_2$ was stable up to 770 K at the highest NO partial pressures employed. Phase I transformed into the amorphous intermediate phase II, which contained mainly nitrate and nitrite ions and Ba-nitrito species, at higher temperatures, or at lower NO pressures. The next step in the activation was the formation of phase III, which consists of nitrate ions and mainly Ba-nitro

complexes. This phase was stable in decreasing NO pressures until its decomposition into BaO. In pure He, this decomposition occurred already at temperatures as low as 720 K after extended time periods. The phase diagram as determined by in situ Raman spectroscopy is illustrated in Fig. 8B. Most importantly, the formation of phase III, containing mainly the Ba-nitro species, occurred under conditions at which catalytic activity was observed. The decomposition of phase III into defect-rich BaO closely matches the calculated phase boundary between BaO, BaO_2, and $Ba(NO_3)_2$ (Fig. 8B). The sharp decrease in nitro complex Raman intensity and, consequently, the catalytic activity at a particular temperature is difficult to understand by the usual temperature effects on the rate of reaction. The sharp fall-off in catalytic activity appears to
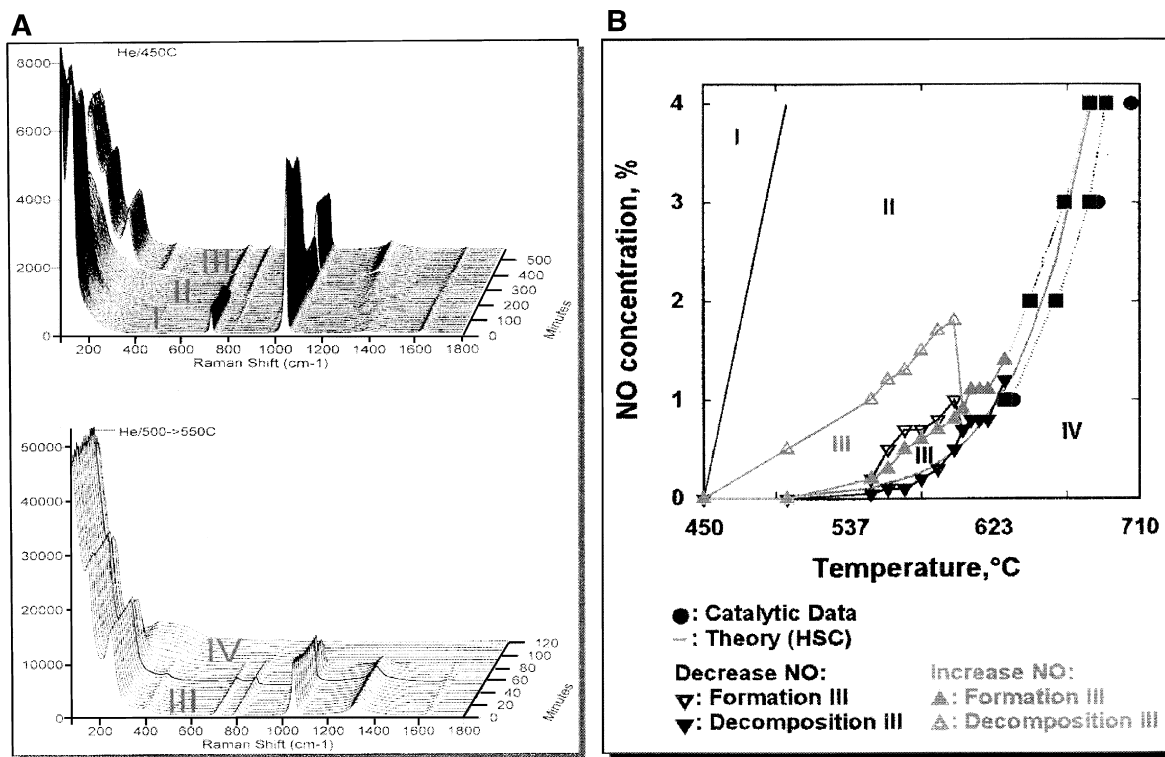

Fig. 8. (A) Time resolved in situ Raman spectra of the activation of 14 mole% Ba/MgO catalyst at 450°C, 500°C and 550°C in flowing He. During activation, four phases were detected. (B) Phase diagram of the four identified phases of 14 mole% Ba/MgO catalysts, determined by in situ Raman spectroscopy, as function of temperature and NO partial pressure (adapted from Ref. [46]).
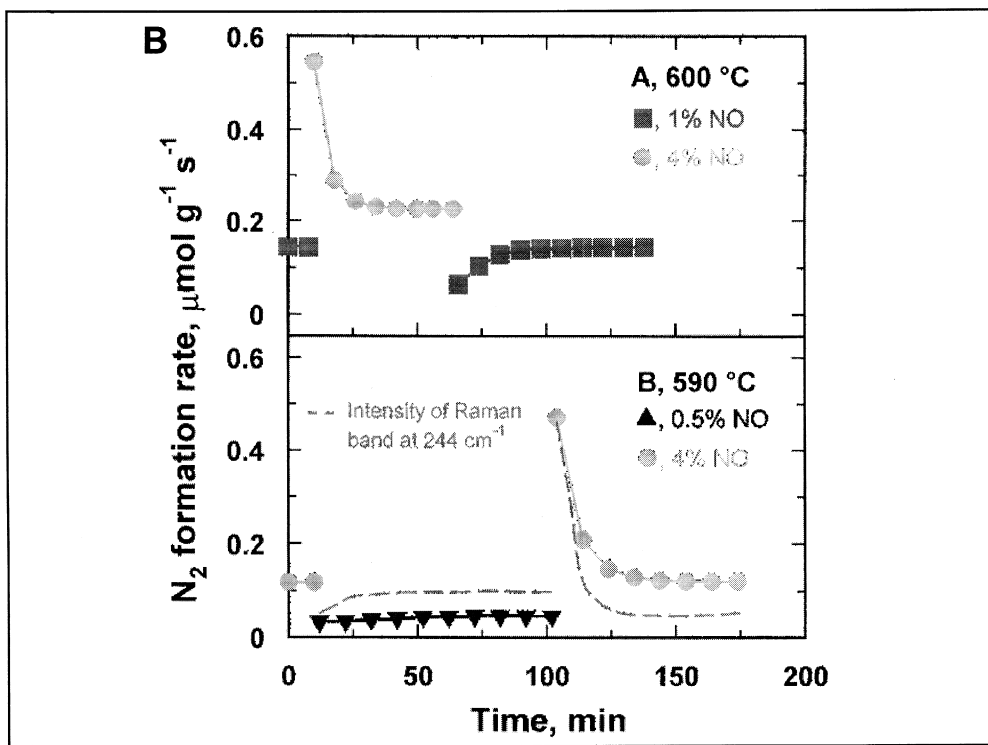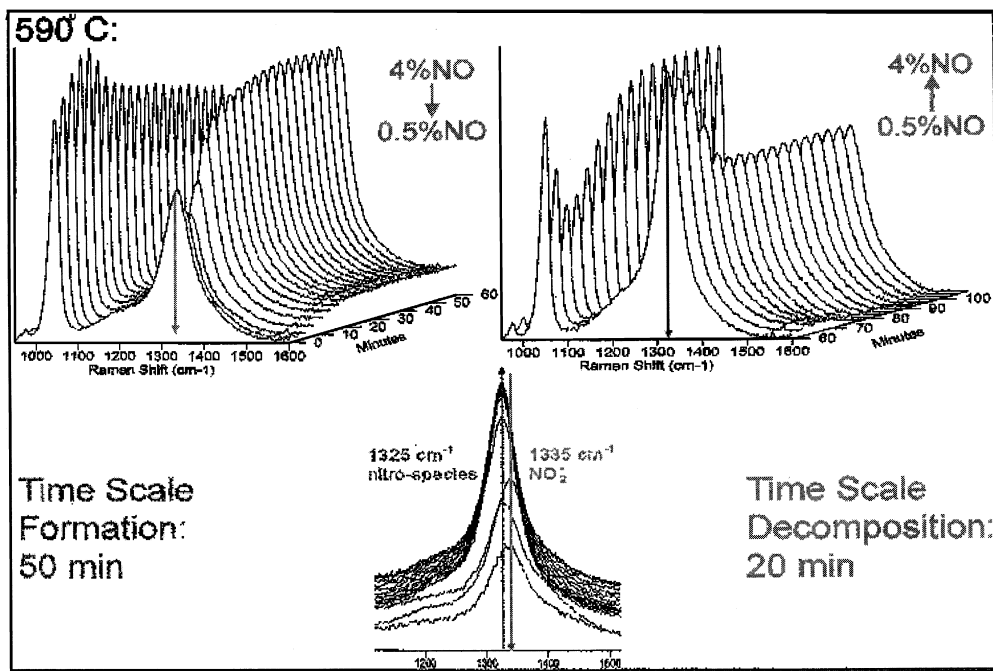
Fig. 9. Time resolved in situ Raman spectra recorded during transient partial pressure step experiments at 590°C (A), revealing the direct correlation between catalytic activity and the intermediate Ba-nitro species (B) (adapted from Ref. [47]).

be related to a phase transition that involves BaO, BaO_2, and $Ba(NO_3)_2$ in relatively large crystallites on the MgO surface.

A comparison between the catalytic and in situ Raman results supports the role of a $Ba-NO_2$ surface intermediate during NO decomposition. This nitro intermediate seems to be responsible for the unusual activity maximum. Transient in situ Raman experiments (Fig. 9) across the phase boundaries convincingly demonstrated that the Ba-nitro complexes show a behavior upon changes in the gas phase NO concentration, which is consistent with the catalytic data: their concentration decreases on the same time scale as the catalytic activity in-

creases and vice versa (Fig. 9). Opposite to that, the intensity variations of the Raman bands of the NO_3- or Ba-nitrito species are not in agreement with the changing catalytic activities. Thus, these species are only indirectly related to the catalytic cycle. The amorphous phase II seems to act as a buffer for the active Ba-nitro intermediates when the NO concentrations above the catalyst are varied.

The characterization of the nitrate Raman bands and those of crystalline barium peroxide led to an interpretation of the observed complex dependence on the O_2 pressure within an overall reaction scheme. Oxygen plays a dual role, as shown in Fig. 10A. It produces barium perox-
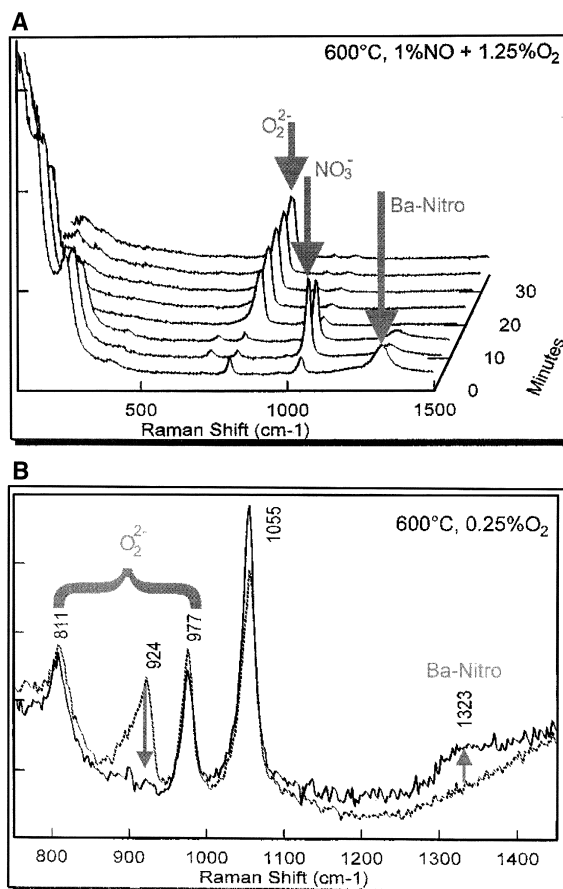

Fig. 10. (A)Time resolved in situ Raman spectra of the reaction of a high O_2 partial pressure with the reactive Ba-nitro intermediate at 600°C. (B) In situ Raman spectra of the reaction of surface peroxide groups, stable at low O_2 partial pressures, with NO at 600°C under formation of the reactive Ba-nitro intermediate.

ide (bands near $800–820$ cm^{-1}), which reacts with NO to give the nitro intermediate. In situ Raman spectroscopy of the decomposition of supported BaO_2 into defect-rich BaO revealed, however, this to occur under O_2 partial pressures, which were at least an order of magnitude higher than those during the catalytic decomposition of NO. BaO_2 was accordingly never detected by Raman spectroscopy under catalytic conditions. Thus, the presence of BaO_2 is not required for NO activation and the formation of Ba-nitro species. Raman spectroscopy evidences the formation of Ba-nitro species via the reaction of NO with surface peroxide ions on defect-rich BaO (Fig. 10B). This peroxide species was identified by its response to changes in the O_2 partial pressure and by ^{18}O isotope labeling and is stable at temperatures up to 1000 K in the presence of O_2 [48]. In addition, the formation of the active phase III from defect-rich BaO required time periods comparable to those needed for catalyst reactivation. This peroxide species on defect-rich BaO, thus, is suggested to be the center, which activates gas phase NO. On the other hand, excessive O_2, being also a reaction product, converts the active nitro species to the inactive nitrate. This oxidation reaction is the reason for the observed inhibiting effect of O_2 on the catalytic NO decomposition.

Lunsford et al. proposed the following catalytic cycle on the basis of these observations: (i) nitric oxide, either from the gas phase or weakly adsorbed on the surface (although not be detected), reacts with a $Ba-NO_2$ intermediate to form N_2 and O_2; (ii) the nitro species are regenerated by the reaction of NO with surface peroxide ions, or alternatively from the decomposition of $Ba(NO_3)_2$; and (iii) molecular oxygen converts nitro species into inactive nitrate ions, but it is also required to generate the nitro intermediate by forming surface peroxides.

Xie and Lunsford [49] showed that N_2O can be decomposed over the same type of catalysts too in the comparable temperature regime above 550°C, however, without showing this pronounced activity maximum, which was ob-served for the NO decomposition. As in case of the NO decomposition an inhibiting effect of additional oxygen in the feed was observed. Small amounts of O_2 added led to a pronounced decrease in the N_2O conversion. In situ Raman spectroscopy was applied in order to elucidate the inhibiting role of oxygen.

In Fig. 11A, the series of time-resolved Raman spectra is shown, which was recorded after switching the gas flow from He to 10% N_2O at 400°C. Catalytic activity was not observed at this temperature. The appearance of bands due to crystalline BaO_2 was observed at 843 cm^{-1} within the first 4 h time on stream. Bands due to $Ba(NO_3)_2$ appeared in the Raman spectra after first crystalline BaO_2 was formed after about 4 h on stream. After very extended reaction times, the Raman bands of $Ba(NO_2)_2$ were observed too.

The same experiment was repeated under catalytic conditions at 500°C (Fig. 11B). Under these conditions, crystalline BaO_2 is not formed anymore. A band at 932 cm^{-1}, however, grows in intensity on a time scale, which is identical to the reduction of the N_2O conversion. This Raman band was assigned to peroxide defects on the surface of defect-rich BaO. Inverse temporal correlation of the intensity of this band with the reduction of the N_2O conversion hints that the formation of these centers is the direct origin of the loss in activity. The Raman band of Peroxide defects in the bulk of BaO at 983 cm^{-1}, on the other hand, does not show a temporal behavior that is related to the change in activity.

To further prove the interrelation of the band intensity of the peroxide defects with the catalytic activity, N_2O partial pressure step change experiments were made. In these experiments the gas phase was switched between a N_2O partial pressure of 5 and 20%. When the concentration was increased from 5% to 20% N_2O an overshoot in the N_2 formation rate was observed, which leveled off on the time scale of about 5 min. The opposite behavior was detected when decreasing the N_2O concentration from 20% to 5% (Fig. 11C).
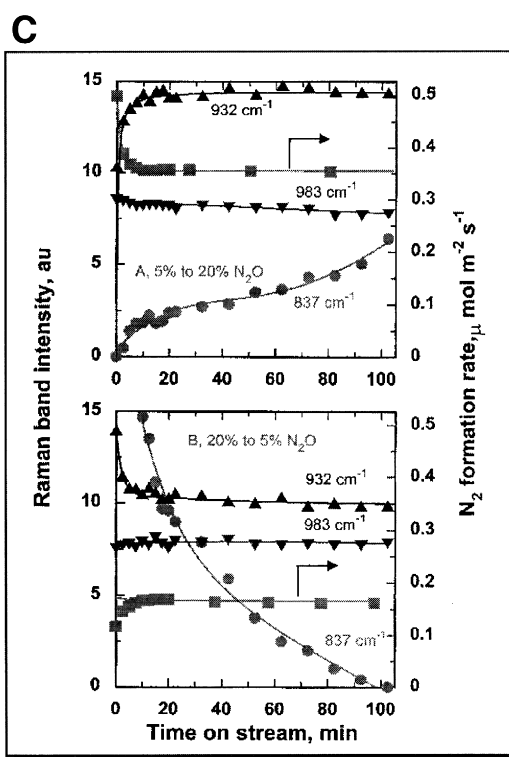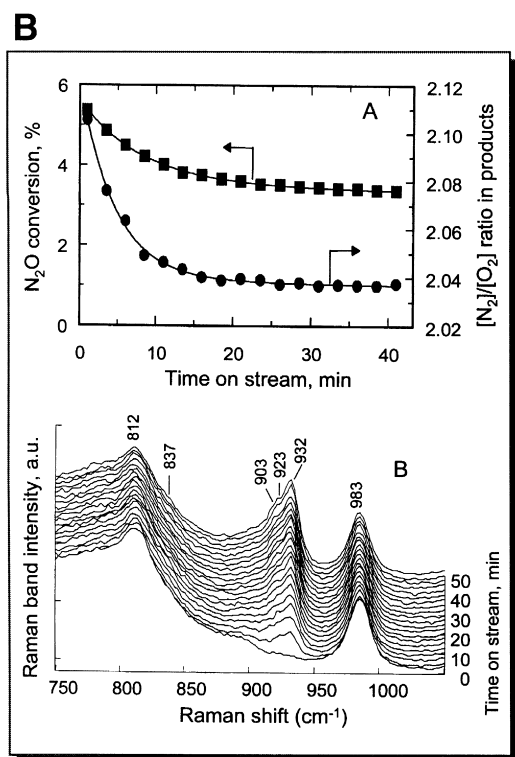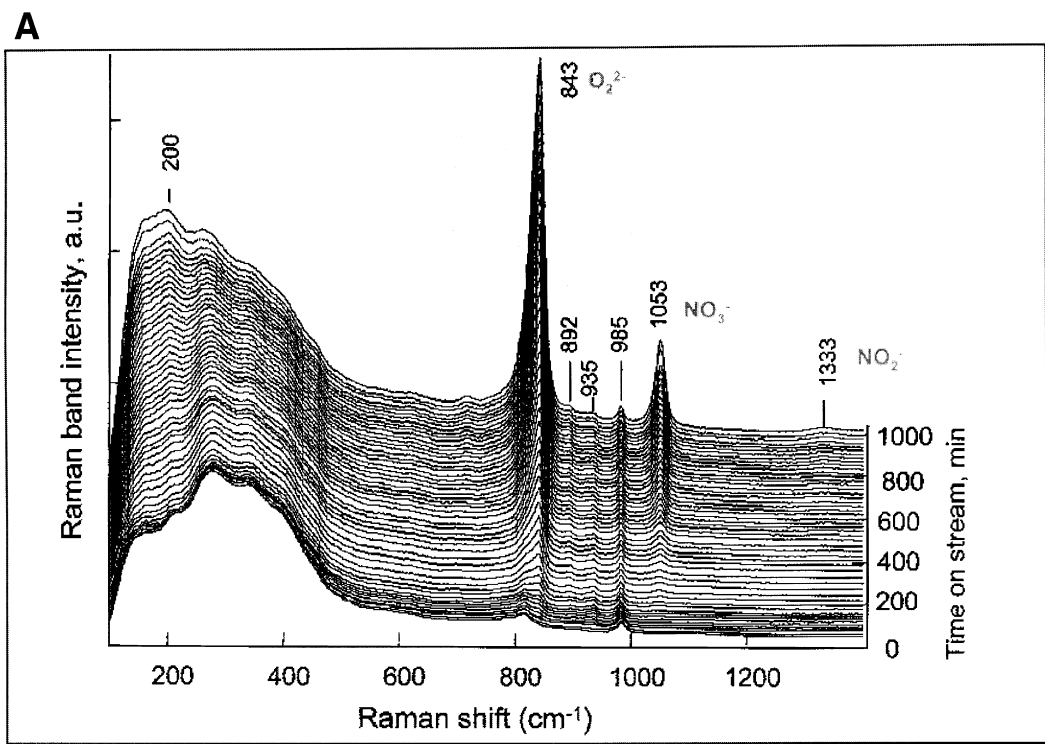
Only the Raman band at 932 cm^{-1} assigned to peroxide defects at the surface of BaO exhibited a temporal behavior, which showed an inverse correlation with the N_2 formation rate on the same time scale. The Raman bands of all other peroxide species exhibited a different temporal behavior. Thus, the deactivation of the catalyst when switching to higher N_2O concentrations must be explained by the increased formation of O_2 and therefore surface peroxide groups on BaO.

From this series of experiments, Xie and Lunsford suggested the following reaction steps of the N_2O decomposition:

1. N_2O reacts with surface O^{2-} ions to give N_2 and surface O_2^{2-};
2. Two surface O_2^{2-} species react to give O_2 and two surface O^{2-} ions;
3. O_2 can react with two surface O^{2-} ions to give the inactive O_2^{2-}.

5. Summary

Raman spectroscopy is certainly one of the most powerful techniques for the characterization of supported metal oxide catalysts. The advantages Raman spectroscopy has, as compared to other techniques, e.g. easy construction of real in situ Raman reactors, high reaction temperatures, usually are no problem, no interference of the gas phase or the support, overweigh by far its few disadvantages, like the occasionally occurring fluorescence, or its inherently low sensitivity.

The new generation of Raman spectrometers render possible time resolved in situ characterization of catalyst activation or even catalytic processes due to their high stability and high light throughput.

Thus, Raman spectroscopy is perfectly suited for the characterization of structural changes occurring in catalytic materials during their action because this vibrational technique is sensitive to crystalline, amorphous, glassy or molecular species. Thus, phase transitions, decompositions, or solid state reactions between different phases present can easily be characterized.

For example, it was shown by in situ Raman spectroscopy that there is no detectable oxygen exchange between MoO_3 and Sb_2O_4 as postulated by the remote control mechanism of selective partial oxidation. Thus, spillover oxygen must be present in very small concentrations probably as a weakly adsorbed surface species. Molecular surface Mo species drastically change their structure and geometry in absence of water from, e.g. polymeric clusters to monomeric highly distorted species. This structural change certainly affects the catalytic properties of such materials. Even crystalline MoO_3 becomes mobile at its Tammann temperature, as proven by in situ Raman spectroscopy, and spreads over support oxides driven by the reduction of the overall surface free energy. Such phenomena certainly occur during catalytic action and may lead to a continuing alteration of the catalytic material, e.g. particle sintering, or disintegration and phase separations as shown by laterally resolved confocal Raman microspectroscopy of a MoVW mixed oxide catalyst for selective partial oxidation.

Fig. 11. (A) Time resolved in situ Raman spectra of the transient reaction of N_2O with 14 mole% BaO/MgO catalyst at 400°C. (B) Time resolved in situ Raman spectra of the transient reaction of N_2O with 14 mole% BaO/MgO at 500°C (lower image). Inhibiting oxygen effect on the conversion of N_2O at 500°C with time on stream (upper image). (C) Direct inverse correlation of the Raman intensity of the surface peroxide groups (band at 932 cm^{-1}) and the N_2 formation rate during transient partial pressure step experiments (upper image: increasing from 5% to 20% N_2O, lower image: decreasing from 20% to 5% N_2O) proving the inhibiting effect of oxygen. The Raman bands of the other peroxide species detected (bands at 983 and 837 cm^{-1}) do not show a temporal behavior correlated with the changing catalytic activity (Figures are courtesy of S. Xie).

Real in situ Raman characterization under catalytic conditions was able to unravel the reaction networks of the direct NO and N_2O decomposition over Ba/MgO catalysts, thus convincingly showing the power of this technique for the study of active catalytic materials.

Due to its broad applicability, Raman spectroscopy will increasingly be used in the near future to characterize catalytic materials under action, to unravel the actual catalytically active species, to follow catalyst deactivation processes, and, hence, to control catalytic reactors at the operation maximum. Fiber optics increasingly will be exploited to record Raman spectra in real catalytic reactors at different positions in the catalyst bed. In addition, variation of the excitation frequency will show resonance effects with electronic transitions and improve our understanding of defect centers, and hence electron transport properties, in catalytic materials.

6. Uncited reference

24

Acknowledgements

References

[1] J.R. Bartlett, R.P. Cooney, in: R.J.H. Clark, R.E. Hester (Eds.), Spectroscopy of Inorganic-Based Materials, Advances in Spectroscopy Vol. 14 Wiley, Chichester, 1987, p. 187.

[2] M. Mehicic, J.G. Grasselli, in: J.G. Grasselli, B.J. Bulkin (Eds.), Analytical Raman Spectroscopy, Wiley, Chichester, 1991, p. 325.

[3] L. Dixit, D.L. Gerrard, H.J. Bowley, Appl. Spectrosc. Rev. 22 (1986) 189.

[4] I.E. Wachs, F.D. Hardcastle, Catalysis Vol. 10 Royal Society of Chemistry, Cambridge, 1993, p. 102.

[5] E. Garbowski, G. Coudurier, in: B. Imelik, J.C. Vedrine (Eds.), Catalyst Characterization. Physical Techniques for Solid Materials, Plenum, New York, 1994, p. 45.

[6] G. Mestl, H. Knözinger, in: G. Ertl, H. Knözinger, J. Weitkamp (Eds.), Handbook of Heterogeneous Catalysis Vol. 2 Wiley-VCh, Weinheim, 1997, p. 539.

[7] G. Mestl, T.K.K. Srinivasan, Catal. Rev. Sci. Eng. 40 (1998) 451.

[8] M. Cardona, in: M. Cardona (Ed.), Topics in Applied Physics, Vol. 8, Light Scattering in Solids I, 2nd edn., Springer, Berlin, 1983, p. 1.

[9] S. Webster, D.A. Smith, D.N. Batchelder, Spectrosc. Eur. 10 (1998) 22.

[10] J.J. Freeman, J. Heaviside, P.J. Hendra, J. Prior, E.S. Reid, Appl. Spectrosc. 35 (1981) 196.

[11] S. Chan, A.T. Bell, J. Catal. 98 (1984) 453.

[12] N. Zimmerer, W. Kiefer, Appl. Spectrosc. 28 (1974) 279.

[13] T.P. Snyder, G.C. Hill Jr., J. Catal. 132 (1991) 536.

[14] P. Knoll, R. Singer, W. Kiefer, Appl. Spectrosc. 44 (1990) 776.

[15] V. Deckert, W. Kiefer, Appl. Spectrosc. 46 (1992) 322.

[16] D. Spielbauer, Appl. Spectrosc. 49 (1995) 650.

[17] J. Hendra, H. Mould, Int. Lab. (1988) 34.

[18] B.C. Chase, Anal. Chem. 59 (1987) 881A.

[19] C. Li, P.C. Stair, Catal. Lett. 36 (1995) 119.

[20] S. Brückner, H. Jeziorowski, H. Knözinger, Chem. Phys. Lett. 105 (1984) 218.

[21] A. Deffontaine, M. Bridoux, M. Delhaye, E. Da Silva, W. Hug, Rev. Phys. Appl. 19 (1984) 415.

[22] J.M. Tedesco, H. Owen, D.M. Pallister, M.D. Morris, Anal. Chem. 65 (1993) 441.

[23] B. Chase, Appl. Spectrosc. 48 (1994) 14A.

[24] A. Otto, Topics in Applied Physics, Vol. 54, Light Scattering in Solids IV, Springer, Berlin, 1984, p. 289.

[25] R.B. Quincy, M. Houalla, D.M. Hercules, J. Catal. 106 (1987) 85.

[26] J.R. Baltrus, L.E. Makovsky, J.M. Stencel, D.M. Hercules, Anal. Chem. 57 (1985) 2500.

[27] P. Ruiz, B. Delmon, Catal. Today 3 (1988) 199.

[28] G. Mestl, P. Ruiz, B. Delmon, H. Knözinger, J. Phys. Chem. 98 (1994) 11269.

[29] G. Mestl, P. Ruiz, B. Delmon, H. Knözinger, J. Phys. Chem. 98 (1994) 11276.

[30] G. Mestl, P. Ruiz, B. Delmon, H. Knözinger, J. Phys. Chem. 98 (1994) 11283.

[31] H. Hu, I.E. Wachs, S.R. Bare, J. Phys. Chem. 99 (1995) 10897.

[32] Y. Lie, C. Xie, Z. Li, Y. Zou, Y. Tang, J. Catal. (China) 5 (1984) 234.

[33] R. Margraf, J. Leyrer, H. Knözinger, E. Taglauer, Surf. Sci. 189/190 (1987) 842.

[34] G. Kisfaludi, J. Leyrer, H. Knözinger, R. Prins, J. Catal. 130 (1991) 192.

[35] J. Leyrer, D. Mey, H. Knözinger, J. Catal. 124 (1990) 349.

[36] G. Mestl, N.F.D. Verbruggen, F.C. Lange, B. Tesche, H. Knözinger, Langmuir 12 (1996) 1817.

[37] G. Mestl, H. Knözinger, Langmuir 14 (1998) 3964.

[38] H. Knözinger, E. Taglauer, Catalysis Vol. 10 Royal Society of Chemistry, Cambridge, 1993, p. 1.

[39] H. Knözinger, E. Taglauer, in: G. Ertl, H. Knözinger, J.

Weitkamp (Eds.), Handbook of Heterogeneous Catalysis Vol. 1 Wiley-VCh, Weinheim, 1997, p. 216.

[40] M.A. Py, K.A. Maschke, Physica 105B (1981) 376.

[41] C. Bremard, P. Dhamelincourt, J. Laureyns, G. Turrell, Appl. Spectrosc. 39 (1985) 6.

[42] H. Adkins, W.R. Peterson, J. Am. Chem. Soc. 53 (1931) 152–1520.

[43] G. Mestl, R. Gottschall, M. Dieterle, Ch. Linsmeier, J. Find, D. Herein, J. Jâger, Y. Uchida, R. Schlôgl, submitted to Appl. Catal. A.

[44] I.R. Beattie, T.R. Gilson, J. Chem. Soc. A (1969) 2322.

[45] S. Xie, G. Mestl, M.P. Rosynek, J.H. Lunsford, J. Am. Chem. Soc. 119 (1997) 10186.

[46] G. Mestl, M.P. Rosynek, J.H. Lunsford, J. Phys. Chem. B 101 (1997) 9321.

[47] G. Mestl, M.P. Rosynek, J.H. Lunsford, J. Phys. Chem. B 101 (1997) 9329.

[48] G. Mestl, M.P. Rosynek, J.H. Lunsford, J. Phys. Chem. B 102 (1998) 154.

[49] S. Xie, J.H. Lunsford, Proc. 16th Meeting of the North American Catalysis Society, 30 May to 4 June 1999, Boston, p. 149.